ELSEVIER

Decoupling photochemical Fe(II) oxidation from shallow-water BIF deposition

Kurt O. Konhauser [a,*], Larry Amskold [a], Stefan V. Lalonde [a], Nicole R. Posth [b], Andreas Kappler [b], Ariel Anbar [c]

[a] *Department of Earth and Atmospheric Sciences, University of Alberta, Edmonton, Alberta, Canada T6G 2E3*
[b] *Center for Applied Geosciences, University of Tuebingen, 72076 Tuebingen, Germany*
[c] *School of Earth and Space Exploration and Department of Chemistry and Biochemistry, Arizona State University, Tempe, Arizona, 85287-1404, USA*

Abstract

Oxidized Fe minerals in Archean–Paleoproterozoic banded iron formations (BIFs) are commonly taken to indicate the presence of biogenic O_2 or photosynthetic Fe(II)-oxidizing bacteria in the oceans' photic zone. However, at least one viable abiogenic oxidation mechanism has been proposed. Prior to the rise of atmospheric oxygen and the development of a protective ozone layer, the Earth's surface was subjected to high levels of ultraviolet radiation. Bulk ocean waters that were anoxic at this time could have supported high concentrations of dissolved Fe(II). Under such conditions, dissolved ferrous iron species, such as Fe^{2+} and $Fe(OH)^+$, would have absorbed radiation in the 200–400 nm range, leading to the formation of dissolved ferric iron [Fe(III)], which in turn, would have hydrolyzed to form ferric hydroxide [Fe(OH)$_3$] at circumneutral pH [Cairns-Smith, A.G., 1978, Precambrian solution photochemistry, inverse segregation, and banded iron formations. Nature 76, 807–808; Braterman, P.S., Cairns-Smith, A.G., and Sloper, R.W., 1983, Photo-oxidation of hydrated Fe^2-Significance for banded iron formations. Nature 303, 163–164]. This process has been invoked to account for BIF deposition without need for biology [François, L.M., 1986, Extensive deposition of banded iron formations was possible without photosynthesis. Nature 320, 352–354]. Here, we evaluate the potential importance of photochemical oxidation using a combination of experiments and thermodynamic models. The experiments simulate the chemistry of ambient Precambrian seawater mixing with Fe(II)-rich hydrothermal fluids with, and without, UV irradiation. We find that if Fe(II) was effused from relatively shallow seamount-type vent systems directly into an anoxic photic zone, the photochemical contribution to solid-phase precipitation would have been negligible. Instead, most of the Fe(II) would have precipitated rapidly as an amorphous precursor phase to the ferrous silicate mineral greenalite ((Fe)$_3$Si$_2O_5$(OH)$_4$), and/or the ferrous carbonate, siderite (FeCO$_3$), depending on different simulated atmospheric pCO_2 levels. Conversely, in experiments where Fe(II) was exposed either to phototrophic Fe(II)-oxidizing bacteria or to O_2, ferric hydroxide formed rapidly, and the precipitation of ferrous iron phases was not observed. If, as suggested on mass balance grounds, BIF deposition requires that Fe be sourced from shallow seamount-type systems, then we are driven to conclude that oxide-facies BIF are the

* Corresponding author. Tel.: +1 780 447 0735; fax: +1 780 492 2030.
E-mail address: kurtk@ualberta.ca (K.O. Konhauser).

product of a rapid, non-photochemical oxidative process, the most likely candidates being direct or indirect biological oxidation, and that a significant fraction of BIF could have initially been deposited as ferrous minerals.

1. Introduction

Banded iron-formations are iron rich (~ 20–40 wt.%) and siliceous (~ 40–60 wt.% SiO_2) sedimentary deposits that precipitated throughout much of the late Archean (2.7–2.5 Ga) and Paleoproterozoic (2.5–1.8 Ga). The "Superior" type BIFs, including those in the Hamersley Group, Western Australia and the Transvaal Supergroup, South Africa, are hundreds of meters thick, over 10^5 km^2 in areal extent, and contain $>10^{13}$ t of iron [1,2]. The source of ferrous iron to the oceans was almost certainly hydrothermal (e.g., [3,4]), but there are considerable uncertainties about the proximity of this source to BIF depositional settings. Holland [5] first proposed that Fe(II) was brought from the deep ocean onto the outer continental shelf by upwelling currents. In this case, the Fe source could have been distal mid-ocean-ridge (MOR) systems. This then led to a depositional model suggesting that BIFs formed below wave base on partially isolated, submerged platforms on the continental shelves of older cratons, where deep ocean water was able to circulate freely into and out of them, but some form of physical barrier was nonetheless required to explain the absence of terrigenous siliciclastic sediment coarser then clay size [6,7]. However, this model for BIF deposition is problematic because it necessitates an upwelling rate on the order of 3000 m yr^{-1} to account for BIF sedimentation rates (based on the Trendall [8] estimate of the amount of Fe in an annual microband; 3×10^{13} g Fe yr^{-1}), if we assume that the concentration of Fe(II) was ~ 0.03 mM, as dictated by equilibrium with siderite and calcite [9]. This upwelling rate is an order of magnitude higher than the maximum rates observed in some modern coastal environments (~ 1 m day^{-1}; [10]).

More recently, it has also been proposed that Fe(II) was directly supplied from hydrothermal plumes to waters as shallow as 300–1000 m [11], similar to Loihi, Hawaii, today [12]. Indeed, Isley and Abbott [13] have suggested a direct link between mantle plume activity between 3.8 and 1.8 Ga and global BIF deposition. This view is supported by the work of Barley et al. [14,15] who proposed that the Hamersley BIF formed during a major tectono-magmatic event that caused an increased supply of dissolved Fe(II) to the oceans. To some extent

this correlates well with sedimentological and petrographic work on the 2.5 Gyr Brockman Iron Formation of the Hamersley Group which suggests that the Fe layers formed as pelagic muds on the flanks of submarine volcanoes, and were later re-sedimented and spread laterally by density currents to a deep water depositional setting, i.e., the trailing continental margin of the Pilbara craton [16,17]. While the actual concentration of dissolved Fe(II) released is unknown, given the elevated temperatures of water–rock reactions in the Archean, it is possible that dissolved Fe(II) in hydrothermal effluents may have been 1–2 orders of magnitude higher than today [18]; the concentration of Fe(II) effused from some modern deep sea vents is 1.8 mM, or ~ 100 mg L^{-1} [19]. Furthermore, the observation that Archean shales are enriched in Fe further indicates a larger hydrothermal flux of Fe to the early oceans [20].

The mechanism by which Fe(II) was oxidized to form BIF is also highly uncertain. Oxidation by photosynthetically produced O_2 is one possibility, allowing for the indirect biological precipitation of ferric hydroxide, Fe(OH)$_3$. Under an anoxic atmosphere, this O_2 could have been confined to localized "oxygen oases" associated with cyanobacterial blooms in coastal settings [21,22]. Cloud further proposed that the primitive O_2-producing bacteria may have lacked suitably advanced oxygen-mediating enzymes, and thus required ferrous iron to detoxify oxygen. If so, these microorganisms would have flourished specifically when Fe(II) and nutrients were made episodically available. Garrels et al. [23] and Hartmann [24] subsequently suggested that light, not O_2, may have coupled the carbon and iron cycles, via photosynthesis that used Fe(II) rather than H_2O as an electron donor, producing Fe(III) rather than O_2. Since then, a number of experimental studies have confirmed that various purple and green bacteria can use Fe(II) as a reductant for CO_2 fixation (e.g., [25]). By modelling photosynthetic Fe(II) oxidation rates, some have even suggested that such microorganisms could have accounted for all of the Fe(III) initially deposited in primary BIF sediment [26,27].

As an alternative to these biological models for Fe(II) oxidation, Cairns-Smith [28] proposed that ferrous iron could have been photooxidized by the high flux of

ultraviolet photons that would have reached the Earth's surface prior to the rise of atmospheric oxygen and the development of a protective ozone layer. This reaction proceeds readily in acidic waters exposed to UV wavelengths in the range of 200–300 nm (reaction 1).

$$2Fe^{2+}_{(aq)} + 2H^+ + h\nu \rightarrow 2Fe^{3+}_{(aq)} + H_2\uparrow \qquad (1)$$
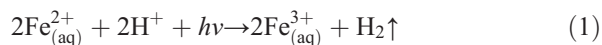
Braterman et al. [29] explored the viability of the photochemical oxidation model at circumneutral pH and over a range of UV wavelengths (217 nm to 406 nm). Based on a quantum yield determined from proton flux, they suggested that at pH > 6.5 the presence of the dissolved ferrous iron species $Fe(OH)^+$ is important because it is oxidized by photons of $\lambda = 300$–450 nm, a wavelength region where the solar flux is more intense and where seawater is more transparent, as compared to $\lambda < 300$ nm. The dissolved ferric iron formed is subsequently hydrolyzed and precipitated as ferric hydroxide. Extrapolating from these experiments, a mean photochemical oxidation rate of 0.5 mol Fe(II) m^{-2} yr^{-1} has been estimated at very rapid upwelling rates (4000 m yr^{-1}), indicating that this process alone could have accounted for up to 1.8×10^{14} mol Fe(III) annually [30]. Other estimates place the total amount of Fe(II) photooxidized annually at 2.3×10^{13} mol [31]. These rates are much greater than that predicted to have precipitated annually as BIF sediment during deposition of the largest such Archean–Paleoproterozoic formations (see [9]). Anbar and Holland [32], noting the relative absence of Mn in BIF, extended these experiments and models to include plausible Archean ocean concentrations of Mn as well as Fe. They found that Mn(II) photooxidizes much more slowly than Fe(II) due to dependence on light with $\lambda < 250$ nm. Hence, the lack of Mn in BIF is consistent with a photochemical pathway.

Significantly, these earlier photochemical experiments focused on determining the specific rates of Fe (II) photochemical oxidation, and did not simulate the complex, disequilibrium water chemistry representative of seamount-type systems, where Fe supply would have been more than adequate to account for BIF deposition rates. They also did not take into account ambient seawater composition, in which there existed a number of ions available to react with dissolved Fe(II) in the water column. The most realistic experiments were those of Anbar and Holland [32], which included 0.56 M NaCl and buffering to pH ~ 7 by the carbonate system under an atmosphere of $pCO_2 = 10^{-1.7}$ atm. However, these experiments were carried out at, or close to, thermodynamic equilibrium conditions, with [Fe] ~ 0.02 mM. In contrast, the photic zone proximal to a seamount-type

system injecting Fe(II) into seawater would have been profoundly out of equilibrium, with much higher concentrations of dissolved Fe(II). This Fe(II) would have mixed with seawater saturated with respect to amorphous silica and calcite [5,33]. It is certain that such disequilibrium systems would have been characterized by rapid precipitation of a variety of Fe(II) phases, in addition to photochemically- and biologically-produced Fe(III) phases. Therefore, the critical parameters in accounting for oxide-facies BIF in seamount-type systems are the relative rates of Fe(II) oxidation by photochemistry and/or other oxidative mechanisms versus ferrous mineral precipitation.

In this work we evaluate the rate of photochemical Fe(II) oxidation in disequilibrium systems in the context of Archean–Paleoproterozoic BIF deposition. We conducted experiments designed to test the oxidative capacity of UV-A (320–400 nm) and UV-C radiation (200–280 nm) on Fe(II)-rich fluids at near-neutral pH (as per [34]) and saturated with respect to a number of minerals postulated to have been important chemical components of the ancient oceans. An experimental temperature of 40 °C was chosen in accordance with predictions for the late Archean based on O and Si isotopes in ~2.5 Gyr cherts [35,36]; it should be noted that this time was preceded by a period of lower temperatures as indicated by glaciogenic units 2.9 Ga, but the temperature then rebounded through increased methane production [37]. We also ran the experiments with bicarbonate concentrations equivalent to water in equilibrium with atmospheric pCO_2 ranging from $10^{-2.4}$ to $10^{-0.4}$ atm, in order to bracket the proposed values for that time (see [38–41]). Importantly, in silica-rich waters, this range of CO_2 values shifts thermodynamic mineral stability fields from siderite (high CO_2) to Fe(II)-silicates (low CO_2), such as minnesotaite and greenalite, allowing us to compare the relative rates of photochemical Fe(II) oxidation to the precipitation of two important BIF mineral constituents.

2. Methodology

A closed, temperature-controlled, general-purpose incubator was fitted with gas purge lines for up to six reaction vessels, and independent UV-A and UV-C light sources were set up to simulate UV irradiation of a hypothetical Archean ocean. Maximum estimates for Archean UV-A surface irradiance approach ~9 mW cm^{-2} over the entire UV-A spectrum [42]; accordingly, a conservative UV-A intensity of 10 mW cm^{-2} was employed using a 400 W medium pressure mercury

floodlamp (Spectroline UV-400) mounted ~15 cm overhead the reaction vessels (Fig. 1A). UV-C radiation was provided by two side-mounted 15 W low-pressure mercury lamps, variably powered with an in-line dimmer, and calibrated for a UV-C flux of 0.3 mW cm^{-2} (as predicted for the Archean surface; [42]). UV light intensity was measured with an Ocean Optics HR4000 fibre optic spectrometer, and irradiation measurements, performed with the spectrometer placed within the quartz reaction vessels, indicated that attenuation by the vessel walls was negligible. For UV-A only experiments, vessels were laid on their side for maximum solution exposure to the overhead UV-A floodlamp. A spectrum for the experimental conditions is shown in Fig. 1(B); note that the low pressure mercury UV-C bulbs act as line sources centred around 254 nm, while the UV-A floodlamp emits a broader spectrum over the 320–400 nm range.
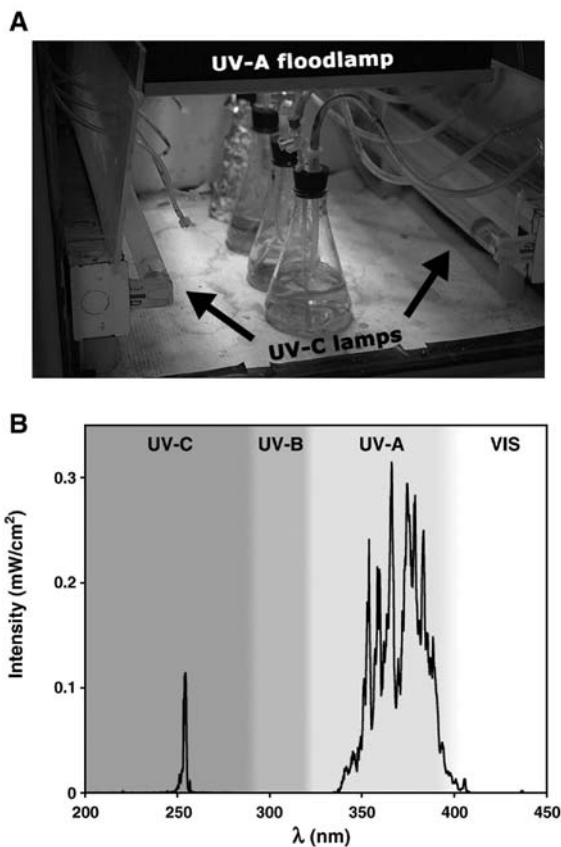

Fig. 1. Depictions of the arrangement (A) and power spectrum (B) of the various UV lights employed for photochemical experiments. The UV-A floodlamp provided 10 mW cm^{-2} integrated over the 320–400 nm range. The UV-C line source was adjusted for a total UV-C intensity of 0.3 mW cm^{-2}. It should be noted that for UV-A experiments, vessels were turned on their side for maximum light exposure.

All experiments were conducted at least in triplicate, in a series of custom-made quartz Erlenmeyer flasks. These reaction vessels were constructed with three ports: a gas outlet, a gas inlet, and a sample port, the latter two extending to the flask bottom via Teflon tubing. The sample port was fitted with a 3-way luer lock valve in order to obtain samples by syringe under anoxic conditions. Experiments were conducted under a constant inert atmosphere (99.99% Ar) delivered via a six-port manifold, and for the actual sampling procedure all solutions were actively bubbled with Ar and magnetically stirred for approximately 15 min.

Various solution chemistries were prepared at seawater ionic strength to give, in addition to NaCl (to adjust ionic strength) and NaOH and HCl (to adjust pH), (1) simple solutions containing only Fe(II), and (2) complex solutions containing Fe(II), HCO_3^-, SiO_2, and Ca^{2+}, designed to more accurately simulate Archean ocean waters:

(1) We performed the Fe(II)-only photochemical oxidation experiments in two different ways. First, in order to allow particle settling and diminish any solution turbidity that may inhibit the photochemical reactions, the gas inlet line was removed from the experimental solutions between sampling points, but continued to deliver Ar at the gas–water interface for positive Ar pressure within the flasks over the duration of the experiments. Second, we conducted experiments with constant agitation (by magnetic stir bars) to assess whether photochemical oxidation was diffusion limited, i.e., if the reactions were confined to a very thin layer, and consequently, the reaction rate was dominated by the rate at which products settled out of that layer versus the rate at which 'fresh' Fe(II) diffuses into this reaction zone.

(2) Three different complex solutions were evaluated, representing solutions in equilibrium with 3 different atmospheres (with pCO$_2$ values of $10^{-0.4}$, $10^{-1.4}$, $10^{-2.4}$) and at saturation with respect to calcite and amorphous silica at pH 7. These experiments were not continuously agitated.

For all solutions, ultrapure water (18.2 MΩ) was first purged of O$_2$ by boiling and cooling to 40 °C with constant N$_2$ bubbling. Salts were added in a stepwise fashion: NaCl (0.56 M) was added first, followed by SiO$_2$ (0.0021 M added as Na$_2$SiO$_3$(H$_2$O)$_9$), Ca^{2+} (added as CaCl$_2$) and HCO$_3^-$ (added as NaHCO$_3$, see Table 1). All reagents were Fisher brand certified A.C.S. Between

each salt addition, the pH was adjusted to between 7.0–7.5 with NaOH or HCl. Following the addition of all aforementioned salts, or after the addition of NaCl in the case of solutions with Fe(II) only, Fe(II) was added (as $Fe(NH_4)_2(SO_4)_2(H_2O)_6$) to yield a solution of approximately 1.8 mM (or ~ 100 mg L^{-1}) Fe(II), similar to the concentration of Fe(II) presently effusing from some modern deep-sea vents [19]. The pH was buffered to between 7.0–7.5 as above, and ~ 200 ml of solution was transferred via syringe to each reaction vessel (pre-purged and at positive pressure with Ar). For selected UV-A experiments, the initial pH was set to be higher than 7.0 (up to 8.0) in order to maximize the potential oxidizing effects of UV-A [29], while remaining below amorphous ferrous hydroxide Fe(OH)$_2$ saturation.

The pH of samples was measured directly in the reaction vessels using an Orion Ross pH electrode calibrated between 3.0 and 10.0 with commercial buffers. Samples (~ 10 ml) were removed periodically by syringe and filtered to 0.2 µm by in-line nylon syringe filters into glass vials containing 3 drops of concentrated HCl. Aliquots of acidified sample were immediately diluted, and Fe(II) and Fe(III) concentrations were determined spectrophotometrically (Beckman-Coulter DU540) within 30 min of sampling by the ferrozine method (after [43]). We chose this method because it allowed us to differentiate ferrous Fe versus ferric Fe (compared to measuring total Fe). The concentration of dissolved silica was determined spectrophotometrically using the heteropoly blue method [44]. UV-free controls were performed exactly as above, but the UV lamps remained off. All experiments were maintained at 40 °C by the incubator's temperature controller. Selected experiments were purged with air instead of Ar to represent rapid oxidation by O$_2$.

Mineral products were isolated for analysis by syringe-filtering fluid samples (obtained as above) onto 0.2 µm Nylon in-line filters, and drying the filters under a constant stream of Ar. X-ray diffraction (XRD) analyses were performed on powdered samples using a Rigaku Geigerflex diffractometer with a Co source and graphite monochromator. Ferrous iron-containing min-

eral products were additionally examined in their anoxic parent solution (in sealed quartz capillary tubes, without filtering and drying) using a Bruker D8 Discover micro-XRD system with a Cu source and a Bruker HiStar GADDS detector. Powdered samples were also examined using a JEOL 6301F field emission scanning electron microscope (SEM) equipped with a PGT X-ray elemental analyzer, after carbon stub mounting and a ~ 3 nm Au sputter coat (Nanotek SEMprep 2). Finally, the carbon content of selected powdered samples was determined in pressed tin boats using a Costech Instruments elemental combustion system with a Thermo-Finnigan Conflo III interface coupling to a Finnigan Mat Delta Plus Advantage mass spectrometer.

In order to compare rates of photosynthetic Fe(II) oxidation, the Fe(II)-oxidizing microorganisms "*Thiodictyon sp.*" strain F4 and "*Rhodobacter ferrooxidans*" sp. strain SW2 were cultivated at the University of Tuebingen in a fresh-water mineral medium with 2.0 mM dissolved Fe(II) at pH 6.9 and 19 °C, as described previously [45]. Cultures were incubated in triplicate with an abiotic blank at 800 lux with 40 W tungsten incandescent light bulbs as light source. Silica was added to medium containing dissolved Fe(II) in the form of sodium metasilicate nonahydrate ($Na_2O_3Si \cdot 9H_2O$) to a final concentration of 2.0 mM. The cultures were then inoculated with an initial density of 10^7 cells ml^{-1}. Fe(II) and Fe(III) concentrations were determined spectrophotometrically (FlashScan 550, Analytik Jena, Germany) via the ferrozine method (after [43]).

3. Results

3.1. Thermodynamic modelling

In order to assess the effects of hydrothermally-derived Fe(II) effusing directly into shallow marine waters, we modelled (using the visual MINTEQ v. 2.51 software package; [46]) the addition of 1.8 mM Fe(II) to silica- and calcite-saturated solutions in equilibrium with variable pCO$_2$ at pH 7.0 and 40 °C (Table 2). Under all atmospheric pCO$_2$ concentrations, greenalite and siderite are predicted to precipitate, but as pCO$_2$, and hence the concentration of HCO$_3^-$ increases, siderite precipitation becomes more favourable. Calcite and amorphous silica are not predicted to precipitate, as they are modelled to be at saturation. It should be noted, however, that these thermodynamic predictions are subject to two important caveats: (1) saturation indices do not take into account the fact that initial mineral precipitates are often unstable, amorphous phases that are unlikely to be included in thermodynamic databases,

Table 1
Concentrations of Ca^{2+} and HCO_3^- for different atmospheric partial pressures of CO_2 in equilibrium with calcite as calculated by Visual MINTEQ at pH 7.0 and 40 °C

log pCO$_2$ (atm)	Ca^{2+} (mM)	HCO$_3^-$ (mM)
−2.4	4.59	2.40
−1.4	0.49	23.7
−0.4	0.08	233

Table 2
Saturation indices and dominant dissolved Fe(II) species in silica- and calcite-saturated seawater containing 1.8 mM Fe(II) and equilibrated with different partial pressures of atmospheric CO_2

	pCO_2 (atm)		
	$10^{-2.4}$	$10^{-1.4}$	$10^{-0.4}$
	Saturation indices (IAP/K_{sp})		
Siderite	0.76	1.74	2.65
Greenalite	5.92	5.85	5.59
Amorphous silica	0	0	0
Calcite	0	0	0
	% Distribution Fe(II)-species$_{(aq)}$		
Fe^{2+}	88.7	86.0	69.8
$FeCl^+$	8.0	7.8	6.4
$FeHCO_3^+$	0.3	2.6	20.8
$FeOH^+$	0.4	0.4	0.3
$FeSO_4(aq)$	2.6	3.2	2.7

and (2) the kinetics of mineral formation are not considered.

The aqueous speciation of Fe(II) was also modelled for the three concentrations partial pressures of CO_2 and is reported as percentage of total Fe (Table 2). At low atmospheric pCO_2, Fe^{2+} and $FeCl^+$ are the domi-nant Fe(II) species, at 88.7% and 8.0%, respectively, with less than 1% $FeHCO_3^+$ and $FeOH^+$. As pCO_2 concentrations increase from $10^{-2.4}$ to $10^{-0.4}$, the percentage of $FeHCO_3^+$ increases from 0.3% to 20.8%; $FeCl^+$ decreases from 8.0% to 6.4%; and Fe^{2+} decreases from 88.7% to 69.8%. Notably, the concen-tration of $FeOH^+$ is always less than 1% of the total Fe (II) under the conditions modelled. Due to the low concentrations of $Fe(OH)^+$ in solution, only a small fraction of the total iron in our simulated seawater may be photosensitive to UV-A light [29]. As a comparison, at pH ~3, over 99.9% of dissolved Fe(II) will be present in the form of Fe^{2+}.

3.2. Inorganic Fe(II) oxidation experiments

In conjunction with thermodynamic predictions and mineral analyses (see below), we conducted experi-ments to compare the relative rates of abiological/biological Fe(II) oxidation and Fe(II)-mineral precipi-tation (Fig. 2). In the most simple experiments, we subjected solutions with only Fe(II) and NaCl (at pH 7) to either UV-C or UV-A irradiation. In the UV-C ex-periments without agitation, 0.2 mM of dissolved Fe(II) was lost over a 24 h duration, the pH dropped from 7.0
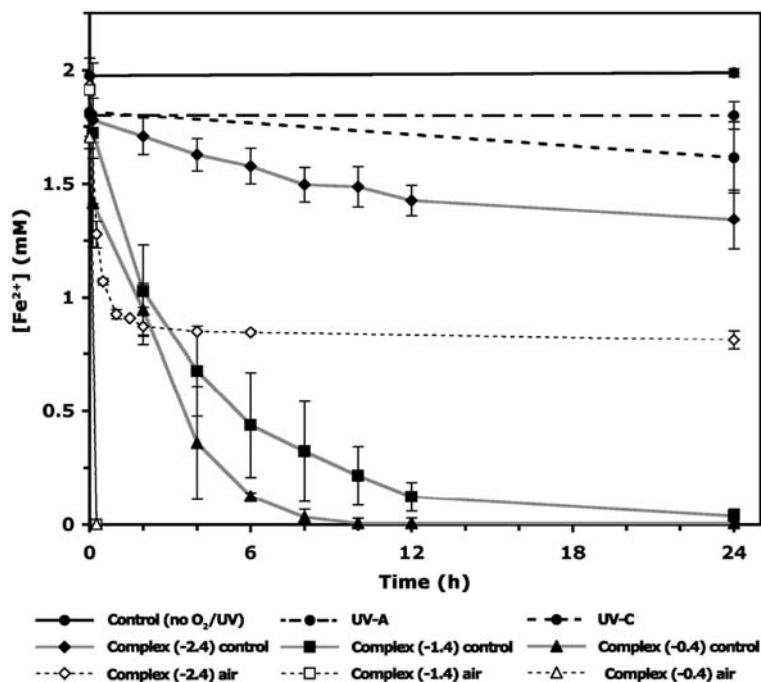

Fig. 2. Experimentally measured concentrations of dissolved Fe(II) for control, photochemical oxidation, mineral precipitation and air-exposed experiments. In the legend, −2.4, −1.4, and −0.4 refer to the log of the pCO_2 equilibrium values used in the experiments. 'Complex control' denotes silica- and calcite-saturated experiments with no irradiation, while "complex air" denotes similar solutions bubbled with air. Continuously agitated Fe(II)-only photooxidation experiments and complex controls exposed to UV are not plotted. Error bars represent 95% confidence intervals.

to ~3.5, and orange-coloured particles formed and settled out to the bottom of the reaction vessel. On occasion a black precipitate formed instead of the typical orange precipitates (see Mineralogy section). Experiments that were constantly agitated showed no increase in iron loss (data not shown), indicating that UV penetration and Fe(II) diffusion over a restricted photoactive zone were not limiting on the scale of our experiments. The orange-coloured particles that formed in the agitated experiments remained in suspension, but had no measurable influence on UV-C penetration as measured through the solution after 24 h of UV exposure. In the UV-A only experiments without agitation, dissolved Fe(II) concentrations did not decrease over the experimental duration, pH dropped less than 1 unit, and no precipitate or colour change was observed. UV-A experiments with agitation showed no difference. It is interesting to note that if excess NaOH was added during the initial pH adjustment, a blue-grey precipitate formed, presumably ferrous hydroxide. UV-shielded controls not exposed to O_2 showed negligible changes in Fe(II) and pH remained relatively constant (within ~0.2 pH units), confirming that the fluids remained anoxic throughout the duration of the experiments.

In comparison to above, in the three silica- and calcite-saturated solutions not exposed to UV, (Fig. 2; 'complex [log pCO_2] control'), the loss of dissolved Fe(II) was exceedingly more rapid. In the least buffered of the three

solutions ($pCO_2 = 10^{-2.4}$), only 4 h were required to observe a similar dissolved Fe(II) loss as in the UV-C experiments after 24 h, but in this case due to Fe(II) mineral precipitation. Under conditions of higher pCO_2 ($10^{-1.4}$ and $10^{-0.4}$), an Fe(II) loss equivalent to 24 h of UV-C irradiation occurred within minutes; Fe(II) concentrations decreased to 0.03 mM in 8 and 24 h at high ($10^{-0.4}$) and intermediate ($10^{-1.4}$) simulated pCO_2, respectively. The pH of the $10^{-2.4}$ and $10^{-1.4}$ pCO_2 solutions remained within 0.2 units of their initial value, while the pH of the $10^{-0.4}$ pCO_2 solution increased from ~7 to ~9, over 24 h.

When the same solutions were exposed to UV-C or UV-A radiation, the amount of dissolved Fe(II) loss was within experimental error of the UV-free controls (data not shown), although the pH dropped slightly upon 24 h of UV-C irradiation. In all cases, light grey- to green-coloured mineral precipitates formed spontaneously following the addition of Fe, and without continuous agitation, they quickly settled to the bottom of the experimental vessels, thereby reducing the initial turbidity that could potentially have inhibited continuous UV penetration. It should be noted, however, that we did not attempt to measure whether the Fe(II) component in the precipitates were subsequently photooxidized, although visual inspection of the filtered solid-phases, before and after several minutes of exposure to atmospheric O_2, strongly indicated (by their spontaneous oxidation) that these minerals were
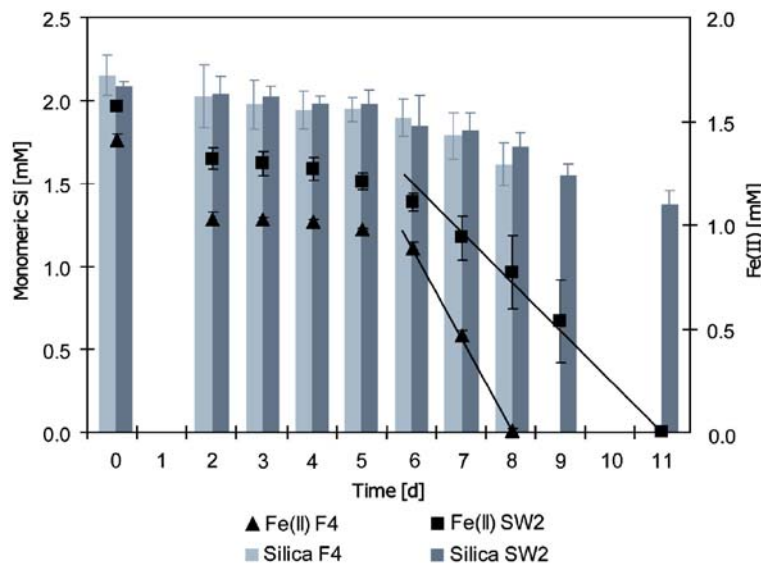

Fig. 3. Oxidation of 2.0 mM dissolved Fe(II) by anoxygenic Fe(II) oxidizing phototrophs *Thiodictyon* sp. F4 (▲) and "*Rhodobacter ferrooxidans*" sp. strain SW2 (■) in the presence of 2.0 mM Si and at light saturation (800 lux). Monomeric silica concentration values measured throughout Fe(II) oxidation are represented by (■) and (■), for *Thiodictyon* sp. F4 and "*R. ferrooxidans*" sp. strain SW2, respectively. Black lines highlight maximum biological Fe(II) oxidation rates. All experiments were performed in triplicate.

predominantly in a reduced form. We also only ran the photochemical oxidation experiments for 24 h, and thus we cannot be fully confident that these minerals would not have been susceptible to subsequent oxidation by continuous UV exposure. Nonetheless, in a natural photic zone setting, one could argue that those precipitates would have settled out of the active UV-C range within a matter of hours: we conservatively estimate the UV photic zone as 100 m thick, based on reasonable penetration depths for 1% UV-A, below which is the aphotic zone; 1% UV-C transmittance is limited to shallower depths, perhaps only 1 m [47].

When the complex solutions were exposed to air (Fig. 2; 'Complex [log pCO$_2$] air'), the initial Fe(II) concentration dropped from ~1.8 mM to 0.002 mM within 15 min in both the $10^{-0.4}$ and $10^{-1.4}$ buffered solutions; this rapid decrease in Fe(II) concentration was accompanied by a distinct orange precipitate. At lower pCO$_2$ ($10^{-2.4}$), Fe(II) concentrations dropped rapidly for the first 4 h, and then remained nearly constant for the remaining 20 h as the pH dropped to a point where Fe(II) oxidation proceeds slowly (pH ~5). The precipitates that formed in low pCO$_2$ experiments exposed to air also had a distinct orange colour, although there was, overall, less solid formed.

3.3. Biological Fe(II) oxidation experiments

The maximum rate of Fe(II) oxidation by anoxygenic Fe(II)-oxidizing phototrophs in the presence of 2.0 mM Fe(II) and 2.0 mM Si was assessed in order to compare the relevant biological processes of Fe(II) oxidation to the abiological reactions reported above. The maximum rates of Fe(II) oxidation by *Thiodictyon* sp. F4 and "*R. ferrooxidans*" sp. strain SW2 under these conditions were 0.6 mM day^{-1} and 0.2 mM day^{-1}, respectively (Fig. 3). These rates increase substantially when the Fe(II) concentration is raised to 4.0 mM, resulting in oxidation rates as high as 2.4 mM Fe(II) day^{-1} by *Thiodictyon* sp. F4 and 0.5 mM day^{-1} by "*R. ferrooxidans*" sp. strain SW2 (data not shown). In all cases, an orange-red solid phase precipitated that showed no crystalline mineral peaks when analyzed by X-ray diffraction. Interestingly, analysis of the supernatant during and after Fe(II) oxidation showed that the Si remained largely in solution as monomeric silica, an observation inconsistent with a number of studies that have demonstrated the high affinity of silica to iron hydroxides (e.g., [48,49]). Although secondary to the focus of this study, this discrepancy is likely attributed to the preferential sorption of organic compounds (i.e., cellular lysates, chelators, or even the

cell wall proper) to the iron mineral surface (e.g., [50]) thus blocking the sorption sites for Si under the culture conditions.

3.4. Mineralogy

As described above, in most reaction vessels exposed to UV, as well as in the UV-free controls containing dissolved bicarbonate and silica, a precipitate formed; only in the simple Fe(II)-only controls (no O$_2$/UV) and those exposed to UV-A only were solids not evident. It should be noted here that if the pH was adjusted to above 8 in the simple-Fe(II) only experiments, a blue precipitate formed that proved to be highly unstable under oxic conditions, turning orange within a minute of exposure to O$_2$, and thus is assumed to be ferrous hydroxide.

Under the experimental conditions (pH ~7) and in the UV-C photooxidized reaction vessels with Fe(II) only, a distinct orange precipitate was observed within 4 h. Upon treatment with NH$_4$-oxalate, all of the Fe in this solid-phase was soluble, indicating the presence of amorphous ferric hydroxide similar to the minerals precipitated in the biological experiments (see above). XRD analysis confirmed the presence of amorphous two-line ferrihydrite (not shown) and SEM images reveal that the precipitate comprised poorly-crystalline, nano-scale flocs of non-uniform size and morphology (Fig. 4A). As mentioned above, a black precipitate occasionally formed during the Fe(II)-only UV-C experiments, and was magnetic, as evidenced by its attraction to the magnetic stir bars. XRD analysis confirmed for these samples the presence of magnetite, and SEM images revealed that the precipitates were similar in appearance to the amorphous two-line ferrihydrite (not shown). In some Fe(II)-only samples, peaks corresponding to lepidocrocite and goethite were also identified by XRD in addition to amorphous two-line ferrihydrite.

With the addition of HCO$_3^-$, Ca^{2+}, and dissolved silica to the experimental iron solutions, and both in the presence and absence of UV radiation, a grey to pale green precipitate formed upon mixing, and developed no obvious orange component after up to 24 h of UV irradiation. Separate mineral precipitation experiments with Fe(II) and HCO$_3^-$ only (and in the absence of UV radiation) yielded precipitates that were grey in colour, and produced XRD patterns corresponding to siderite (reaction 2), or diverse, metastable, amorphous siderite precursors (based on [51]).

$$Fe^{2+} + CO_3^{2-} \rightarrow FeCO_{3(s)} \qquad (2)$$

SEM images further reveal that this solid consists of nanometer-scale aggregates with a platy texture reminiscent of crumpled tissue (Fig. 4B). Similar mineral precipitation experiments were performed with only Fe(II) and silica, resulting in a green precipitate that turned black upon drying, and yielded no identifiable X-ray diffraction peaks. SEM revealed the precipitates to be highly amorphous, nanometer-scale aggregates that
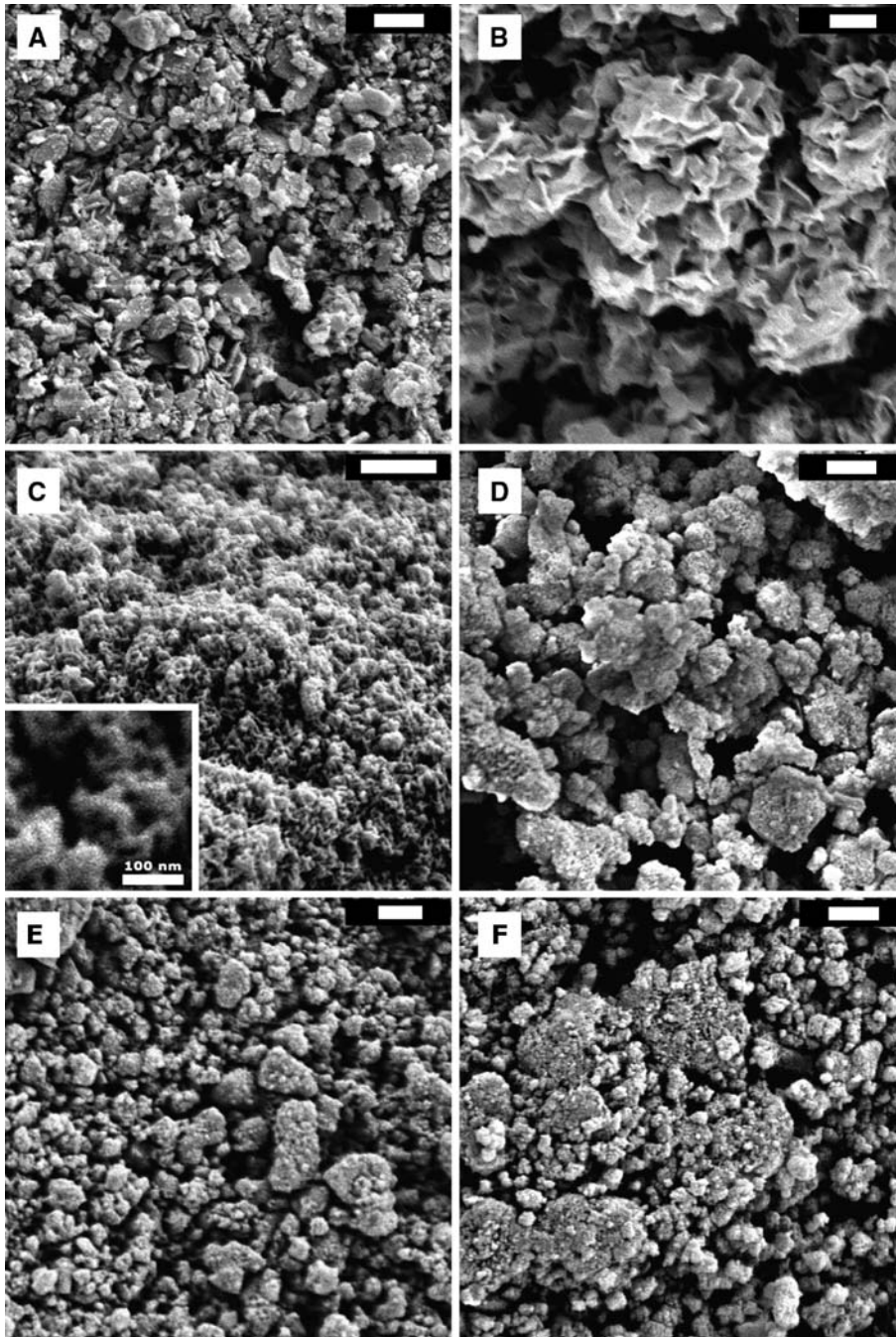

Fig. 4. SEM micrographs of particles precipitated from the various experimental solutions and sampled at 24 h. The following experimental solutions are represented: (A) Fe(II)-only solutions after 24 h of UV-C exposure; (B) iron and bicarbonate solutions without UV exposure; (C) iron and silica solutions without UV exposure; and iron, silica, and bicarbonate solutions representing log atmospheric pCO_2 values of -0.4 (D); -2.4 (E); and -1.4 (F). All scale bars are 500 nm, except the 100 nm scale bar in the inset of (C), which highlights the novel tubular structure of the iron-silicate composite.

possessed a tubular appearance on the smallest visible scale (inset, Fig. 4C). X-ray analyses indicated the presence both Fe and Si, and thermodynamic modelling predicts that all of the silica-containing solutions are highly supersaturated with respect to the ferrous-silicate mineral greenalite (reaction 3):

$$3Fe^{2+} + 2Si(OH)_4 + H_2O \rightarrow Fe_3Si_2O_5(OH)_4 + 6H^+ \qquad (3)$$
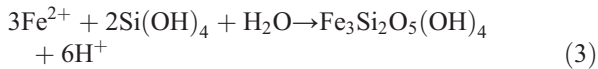
Precipitates obtained from the complex solutions containing Fe, SiO_2, HCO_3^-, and Ca^{2+} were amorphous and unidentifiable by XRD. With aqueous bicarbonate concentrations progressively decreasing (reflecting decreasing atmospheric pCO_2 as discussed above), the accumulation of visible precipitates was slower, and the precipitates themselves were less grey and more pale green in colour. Correspondingly, SEM demonstrates that the precipitates in the $10^{-0.4}$ pCO_2 experiments (Fig. 4D) were similar in aggregate size to the Fe(II)- and HCO_3-only precipitates, while the precipitates in the $10^{-2.4}$ experiment bear a closer resemblance to the Fe(II)- and SiO_2-only precipitates (Fig. 4E); the $10^{-1.4}$ precipitates appear as an intermediate (Fig. 4F). It is interesting that acid-base titrations of particles precipitated from the $10^{-1.4}$ experiments reveal that there is significant dissolution at both low and high pH, possibly indicating the presence of (at least) two mineral phases (data not shown). Based on the composition and saturation indices, we hypothesize that the phase dissolving at low pH is a Fe(II)-carbonate, while the phase dissolving at high pH is a Fe(II)-silicate.

The SEM analyses agree well with preliminary data regarding these solids' composition, which indicate that as pCO_2, and thus HCO_3^-, is increased, the particles incorporate less Si, and more C (with solid phase Si:C molar ratios of 55:1 at $pCO_2 = 10^{-2.4}$ decreasing to 3.8:1 at $pCO_2 = 10^{-0.4}$). It should be noted that the carbon, iron and silicon contents of the dried particles varied considerably between experimental runs, and it is likely that small differences in mixing rates and local geochemical environments (that at the end determine formation of the initial aggregates) might be responsible for the nature and composition of the above-described precipitates.

4. Discussion

During mantle plume events, the eruption of komatiitic and tholeiitic magmas produce relatively shallow oceanic plateaus, aseismic ridges and seamount chains comprised of Fe-rich mineral phases. High temperature water–rock reactions, in the absence of dissolved sulfate,
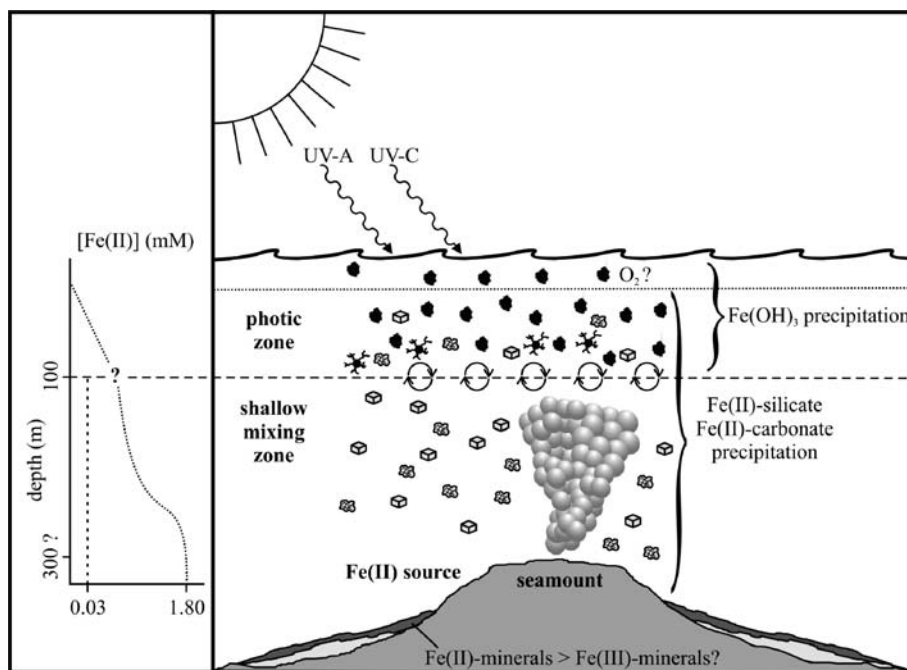

Fig. 5. Conceptual model showing Fe(II) effused from a shallow seamount-type system almost directly into the photic zone of the ocean, where its concentration is diminished by a combination of mineral precipitation, photochemical oxidation, anoxygenic photosynthesis, and possibly reaction with dissolved O_2, which could be present in localized 'oases' or in a continuous surface layer. The attainment of equilibrium conditions depends on the relative depth of the seamount vent versus the depth of the photic zone.

could then foster the release of highly reduced, Fe(II)-rich hydrothermal fluids [18] directly to the upper ocean (e.g., [52,13]), and maybe even the photic zone. Under such conditions, the fate of Fe(II) depends on the competing kinetics of photochemical oxidation, reaction with localized sources of O_2, photosynthetic Fe(II) oxidation, and mineral precipitation (Fig. 5). Although experiments were run for 24 h, here we consider only the first 12 h in order to normalize our rates according to a diel cycle. Our complex solution experiments lose similar amounts of Fe(II) to mineral precipitation irrespective of UV exposure. Dissolved Fe(II) loss is greatest, and most rapid in $pCO_2 = 10^{-0.4}$ solutions, with 1.8 mM of Fe(II) lost, while 1.7 and 0.4 mM of Fe(II) is lost in the same amount of time for $pCO_2 = 10^{-1.4}$ and $10^{-2.4}$, respectively. Over 12 h of UV exposure in Fe(II)-only solutions, Fe(II) loss was ~0.1 mM for UV-C and negligible for UV-A. Clearly our results contradict earlier studies suggesting the importance of UV-A in terms of Fe(II) oxidation at circumneutral pH [29,31,32]. The discrepancy may arise for two reasons:

(1) We employed different light sources. The medium-pressure Hg lamp used by Anbar and Holland [32] gave continuous UV output across the spectrum, with superimposed Hg peaks. In contrast, our experiments have spectral gaps (UV-B, and also wavelengths shorter than 250 nm). UV-B has not been reported as being important for photochemical Fe(II) oxidation, but this spectral region has not been directly tested before. Wavelengths shorter than 250 nm may also be significant because such energetic photons can drive the formation of highly reactive species. For example, in the presence of Cl^-, such short wavelength UV (as in the experiments of Anbar and Holland [32], but not our own) could lead to formation of Cl radicals which are powerful oxidants.

(2) In our experiments we used relatively high dissolved Fe(II) concentrations (1.8 mM) compared to those of Anbar and Holland [32] who used Fe(II) concentrations ranging from 0.003 to 0.2 mM. When we conducted similar photochemical oxidation experiments at lower Fe(II) concentrations we noted a loss of ~0.03 mM Fe(II) (from a starting concentration of 0.08 mM) due to UV-A exposure over 12 h (data not shown). This higher rate of Fe(II) oxidation at lower concentrations is puzzling and requires further study.

The dominance of mineral precipitation over photochemical oxidation in terms of loss of dissolved Fe(II) is not surprising given the state of supersaturation of our experimental fluids. Our solutions were made to mimic possible Archean seawater in the vicinity of hydrothermal venting, where silica concentrations were at least as high as at saturation with cristobalite (0.67 mM at 40 °C in seawater), and possibly even amorphous silica (2.20 mM) [33]. Similarly, in the presence of an atmosphere with pCO_2 values ranging from $10^{-2.4}$ to $10^{-0.4}$ atm, the oceans may have had bicarbonate levels significantly higher than today (e.g., [42]). Such concentrations would have had two effects: (1) it would have led to the rapid precipitation of ferrous carbonate phases and (2) a significant fraction of the aqueous Fe would have been in the form of dissolved Fe(II)-carbonate species (e.g., up to 20.8% as $FeHCO_3^+$ at $pCO_2 = 10^{-0.4}$).

Crucially, our photochemical oxidation results imply that Fe(III) mineral precipitation could not have dominated over Fe(II) mineral precipitation in seamount-type systems unless there existed an oxidative mechanism more rapid than photochemical oxidation. There are two obvious candidates. First, rates of Fe(II) oxidation by O_2 are extremely rapid in modern oxygenated seawater (on the order of minutes in seawater; e.g., [53]), hence, dissolved Fe(II) removal by this reaction is considerably faster than oxidation by UV radiation. We have verified this expectation in control experiments continuously purged with air. In these experiments, Fe(II) loss can be 100% within minutes (recall Fig. 2). For example, at high pCO_2, the elevated buffering capacity of the waters ensures that pH remains sufficiently high that inorganic Fe(II) oxidation proceeds rapidly; at low pCO_2, before all of the ferrous iron can be oxidized, the pH drops to the point where inorganic rates of Fe(II) oxidation are considerably slower. Clearly, if O_2 was available, it would have been an important mechanism of Fe(II) loss. Although we have few constraints on O_2 availability during the late Archean, despite evidence supporting the existence of cyanobacteria at that time (e.g., [54,55]), this classic scenario remains a possibility in localized oxygen oases.

Second, anoxygenic photosynthetic bacteria may have utilized Fe(II) as a reductant. While limited data exist on Fe(II) oxidation rates by anoxygenic bacteria, a recent study by Kappler et al. [27] demonstrated that the purple nonsulfur bacterium, R. ferrooxidans strain SW2, displays a linear dependence on light intensity, up to 600 lux, above which light saturation becomes important. In addition, the metabolic rate of the photoferrotrophs was shown to be dependant upon the available wavelengths of light. Given that wavelengths <300 nm and >600 nm are readily adsorbed or scattered by water within the top few meters of the

ocean, the authors subsequently measured rates of Fe (II) oxidation using only wavelengths <650 nm. They calculated that a photoferrotrophic community, using essentially only their carotenoids for light absorption (at wavelengths between 360–520 nm), could grow at depths of 100 m and oxidize Fe(II) at rates on the order of 0.014 mM day^{-1}. However, when those same bacteria additionally utilize bacteriochlorophyll (as would occur in more shallow waters), their oxidative capacity is increased to 0.4 mM day^{-1}. In this study with the purple sulfur bacterium "Thiodictyon sp." strain F4 and the purple non-sulfur bacterium "R. ferrooxidans" sp. strain SW2 (exposed to the full light spectrum, 2.0 mM Fe(II) and 2.0 mM Si), oxidation rates (0.6 mM day^{-1} and 0.2 mM day^{-1}, respectively) fell within the range of the UV-C photochemical oxidation experiments (0.2 mM day^{-1}) and ferrous mineral precipitation controls (0.5–1.8 mM day^{-1}). When these strains were exposed to 4.0 mM Fe(II) and 2.0 mM Si, however, we found that Fe(II)-oxidation rates of these microorganisms ranged from 0.5 mM day^{-1} to as high as 2.4 mM day^{-1}. This rate is higher than those for both abiological processes. This increase in oxidation rate suggests that these microorganisms may adapt to higher dissolved Fe(II) concentrations, and that microbial oxidation rates could increase with pulses of Fe(II) from hydrothermal vents.

5. Conclusions

At present, much of the consensus on BIF deposition necessitates some form of oxidative mechanism; photochemical oxidation, anoxygenic bacterial photosynthesis or abiological oxidation with cyanobacterially-generated O_2. However, if Fe(II) was effused into shallow waters from a seamount-type system, our experiments suggest that photochemical Fe(II) oxidation would not have been a dominant mechanism for dissolved Fe(II) loss. It is therefore difficult to account for ferric oxide in BIF as primary precipitates without invoking either the presence of dissolved O_2 or Fe(II)-based bacterial photosynthesis — both biologically-associated processes. It is also interesting to note that our observations might challenge the accepted view that much of the Fe(II) component in BIF are predominantly diagenetic (e.g., [7]). Given that BIFs have an average overall oxidation state of Fe$^{2.4+}$ [56] it is plausible that much of the Fe(II) fraction is a primary signature. In fact, some earlier studies have even argued that the siderite-rich deposits in the Kuruman Iron Formation of the Transvaal Supergroup, South Africa are primary precipitates [57] while in the well oxidized portions of the initial Brockman IF sediments, primary

siderite and greenalite were replaced by hematite (Fe$_2$O$_3$) and ankerite (CaFe(CO$_3$)$_2$). In less oxidized portions of the initial sediment, siderite was replaced by magnetite [58]. Clearly, developing a better understanding of the origins of Fe(II) minerals in BIF has important implications for Fe cycling and redox conditions in Archean and Paleoproterozoic oceans.

Acknowledgements

References

[1] A.F. Trendall, The significance of iron-formation in the Precambrian stratigraphic record, Spec. Publ. Int. Assoc. Sedimentol. 33 (2002) 33–66.

[2] C. Klein, Some Precambrian banded iron-formations (BIFs) from around the world: Their age, geologic setting, mineralogy, metamorphism, geochemistry, and origin, Am. Mineral. 90 (2005) 1473–1499.

[3] S.B. Jacobsen, M.R. Pimentel-Klose, A Nd isotopic study of the Hamersley and Michipicoten banded iron formations: the source of REE and Fe in Archean oceans, Earth Planet. Sci. Lett. 87 (1988) 29–44.

[4] M. Bau, P. Möller, Rare earth element systematics of the chemically precipitated component in Early Precambrian iron-formations and the evolution of the terrestrial atmosphere-hydrosphere–lithosphere system, Geochim. Cosmochim. Acta 57 (1993) 2239–2249.

[5] H.D. Holland, The oceans: a possible source of iron in iron-formations, Econ. Geol. 68 (1973) 1169–1172.

[6] R.C. Morris, R.C. Horwitz, The origin of the iron-formation–rich Hamersley Group of Western Australia- Deposition on a platform, Precambrian Res. 21 (1983) 273–297.

[7] R.C. Morris, Genetic modelling for banded iron-formation of the Hamersley Group, Pilbara Craton, Western Australia, Precambrian Res. 60 (1993) 243–286.

[8] A.F. Trendall, Revolution in Earth history, J. Geol. Soc. Aust. 19 (1972) 287–311.

[9] H.D. Holland, The Chemical Evolution of the Atmosphere and Oceans, Princeton University Press, New Jersey, 1984.

[10] W.S. Broecker, T.H. Peng, Tracers in the Sea, Lamont-Doherty Geological Observatory, New York, 1982.

[11] A.E. Isley, Hydrothermal plumes and the delivery of iron to banded iron formation, J. Geol. 103 (1995) 169–185.

[12] D.M. Karl, G.M. McMurtry, A. Malahoff, M.O. Garcia, Loihi Seamount, Hawaii: a mid-plate volcano with a distinctive hydrothermal system, Nature 335 (1988) 532–535.

[13] A.E. Isley, D.H. Abbot, Plume-related mafic volcanism and the deposition of banded iron formation, J. Geophys. Res. 104 (1999) 15461–15477.

[14] M.E. Barley, A.L. Pickard, P.J. Sylvester, Emplacement of a large igneous province as a possible cause of banded iron formation 2.45 billion years ago, Nature 385 (1997) 55–58.

[15] M.E. Barley, A. Bekker, B. Krapež, Late Archean to Early Paleoproterozoic global tectonics, environmental change and rise of atmospheric oxygen, Earth Planet. Sci. Lett. 238 (2005) 156–171.

[16] B. Krapež, M.E. Barley, A.L. Pickard, Hydrothermal and resedimented origins of the precursor sediments to banded iron formations: Sedimentological evidence from the early Palaeo-proterozoic Brockman Supersequence of Western Australia, Sedimentology (2003) 979–1011.

[17] A.L. Pickard, M.E. Barley, B. Krapež, Deep-marine depositional setting of banded iron formation: sedimentological evidence from interbedded clastic sedimentary rocks in early Paleoproterozoic Dales Gorge Member of Western Australia, Sediment. Geol. 170 (2004) 37–62.

[18] L.R. Kump, W.E. Seyfried Jr., Hydrothermal Fe fluxes during the Precambrian: Effect of low oceanic sulfate concentrations and low hydrostatic pressure on the composition of black smokers, Earth Planet. Sci. Lett. 235 (2005) 654–662.

[19] J.M. Edmond, K.L. Von Damm, R.E. McDuff, C.I. Measures, Chemistry of the East Pacific Rise and their effluent dispersal, Nature 297 (1982) 187–191.

[20] L.R. Kump, H.D. Holland, Iron in Precambrian rocks: implications for the global oxygen budget of the ancient Earth, Geochim. Cosmochim. Acta 56 (1992) 3217–3223.

[21] P. Cloud, Significance of the Gunflint (Precambrian) microflora, Science 148 (1965) 27–35.

[22] P. Cloud, Paleoecological significance of the banded iron-formation, Econ. Geol. 68 (1973) 1135–1143.

[23] R.M. Garrels, E.A. Perry Jr., F.T. Mackenzie, Genesis of Precambrian iron-formations and the development of atmospheric oxygen, Econ. Geol. 68 (1973) 1173–1179.

[24] H. Hartman, The evolution of photosynthesis and microbial mats: a speculation on banded iron formations, in: Y. Cohen, et al., (Eds.), Microbial Mats: Stromatolites, Alan Liss, New York, 1984, pp. 451–453.

[25] F. Widdel, S. Schnell, S. Heising, A. Ehrenreich, B. Assmus, B. Schink, Ferrous iron oxidation by anoxygenic phototrophic bacteria, Nature 362 (1993) 834–836.

[26] K.O. Konhauser, T. Hamade, R. Raiswell, R.C. Morris, F.G. Ferris, G. Southam, D.E. Canfield, Could bacteria have formed the Precambrian banded iron formations? Geology 30 (2002) 1079–1082.

[27] A. Kappler, C. Pasquero, K.O. Konhauser, D.K. Newman, Deposition of banded iron formations by anoxygenic photo-trophic Fe(II)-oxidizing bacteria, Geology 33 (2005) 865–868.

[28] A.G. Cairns-Smith, Precambrian solution photochemistry, inverse segregation, and banded iron formations, Nature 76 (1978) 807–808.

[29] P.S. Braterman, A.G. Cairns-Smith, R.W. Sloper, Photo-oxidation of hydrated Fe^{2+}—significance for banded iron formations, Nature 303 (1983) 163–164.

[30] L.M. François, Extensive deposition of banded iron formations was possible without photosynthesis, Nature 320 (1986) 352–354.

[31] P.S. Braterman, A.G. Cairns-Smith, Photoprecipitation and the banded iron-formations — some quantitative aspects, in: P.W.U. Appel, G.L. LaBerge (Eds.), Precambrian Iron-Formations, Theophrastus, Athens, 1986, pp. 221–228.

[32] A.D. Anbar, H.D. Holland, The photochemistry of manganese and the origin of banded iron formations, Geochim. Cosmochim. Acta 56 (1992) 2595–2603.

[33] R.G. Maliva, A.H. Knoll, B.M. Simonson, Secular change in the Precambrian silica cycle: insights from chert petrology, Geol. Soc. Amer. Bull. 117 (2005) 835–845.

[34] J.P. Grotzinger, J.F. Kasting, New constraints on Precambrian ocean composition, J. Geol. 101 (1993) 235–243.

[35] L.P. Knauth, Temperature and salinity history of the Precambrian ocean: implications for the course of microbial evolution, Palaeogeogr. Palaeoclimatol. Palaeoecol. 219 (2005) 53–69.

[36] F. Robert, M. Chaussidon, A palaeotemperature curve for the Precambrian oceans based on silicon isotopes in cherts, Nature 443 (2006) 969–972.

[37] A.A. Pavlov, J.F. Kasting, J.L. Eigenbrode, K.H. Freeman, Organic haze in Earth's early atmosphere: Source of low-^{13}C late Archean kerogens? Geology 29 (2001) 1003–1006.

[38] R. Rye, P. Kuo, H.D. Holland, Atmospheric carbon dioxide concentrations before 2.2 billion years ago, Nature 378 (1995) 603–605.

[39] A.M. Hessler, D.R. Lowe, R.L. Jones, D.K. Bird, A lower limit for atmospheric carbon dioxide levels 3.2 billion years ago, Nature 428 (2004) 736–738.

[40] D.R. Lowe, M.M. Tice, Geologic evidence for Archean atmospheric and climatic evolution: fluctuating levels of CO_2, CH_4, and O_2 with an overriding tectonic control, Geology 32 (2004) 493–496.

[41] H. Ohmoto, Y. Watanabe, K. Kumazawa, Evidence from massive siderite beds for a CO_2-rich atmosphere before ∼1.8 billion years ago, Nature 429 (2004) 395–399.

[42] A. Segura, K. Krelove, J.F. Kasting, D. Sommerlatt, V. Meadows, D. Crisp, M. Cohen, E. Mlawer, Ozone concentrations and ultraviolet fluxes on Earth-like planets around other stars, Astrobiology 3 (2003) 689–708.

[43] E. Viollier, P.W. Inglett, K. Hunter, A.N. Roychoudhury, P. Van Cappellen, The ferrozine method revisited: Fe(II)/Fe(III) deter-mination in natural waters, Appl. Geochem. 15 (2000) 785–790.

[44] L. Clescerl, A. Greenberg, A. Eaton (Eds.), Standard Methods for the Examination of Waters and Wastewaters, 20th Edition, American Public Health Association, Washington, DC, 1999.

[45] A. Kappler, D.K. Newman, Formation of Fe(III)-minerals by Fe (II)-oxidizing photoautotrophic bacteria, Geochim. Cosmochim. Acta 68 (2004) 1217–1226.

[46] Gustafsson, J.P., 2000, Visual MINTEQ [WWW document]. URL http://www.lwr.kth.se/English/OurSoftware/vminteq/ (ver-ified 15 January 2007).

[47] R.C. Smith, K.S. Baker, Optical properties of the clearest natural waters (200–800 nm), Appl. Opt. 20 (1981) 177–184.

[48] C.D. Davis, H.-W. Chen, M. Edwards, Modeling silica sorption to iron hydroxide, Environ. Sci. Technol. 36 (2002) 582–587.

[49] K.O. Konhauser, S.V. Lalonde, L. Amskold, H.D. Holland, Was there really an Archean phosphate crisis? Science 315 (2007) 1234.

[50] B. Gu, J. Schmitt, Z. Chen, L. Liang, J.F. McCarthy, Adsorption and desorption of natural organic matter on iron oxide: mechanisms and models, Environ. Sci. Technol. 28 (1994) 38–46.

[51] C. Jiminez-Lopez, C.S. Romanek, Precipitation kinetics and carbon isotope portioning of inorganic siderite at 25 °C and 1 atm, Geochim. Cosmochim. Acta 68 (2004) 557–571.

[52] J.E. Lupton, A far-field hydrothermal plume from the Loihi Seamount, Science 272 (1996) 976–979.

[53] F.J. Millero, S. Sotolongo, M. Izaguirre, The oxidation kinetics of Fe(II) in seawater, Geochim. Cosmochim. Acta 51 (1987) 793–801.

[54] R. Buick, The antiquity of oxygenic photosynthesis: Evidence for stromatolites in sulphate-deficient Archaean lakes, Science 255 (1992) 74–77.

[55] J.J. Brocks, G.A. Logan, R. Buick, R.E. Summons, Archean molecular fossils and the early rise of eukaryotes, Science 285 (1999) 103–1036.

[56] C. Klein, N.J. Beukes, Time distribution, stratigraphy, and sedimentologic setting, and geochemistry of Precambrian iron-formations, in: J.W. Schopf, C. Klein (Eds.), The Proterozoic Biosphere: A Multidisciplinary Study, Cambridge University Press, Cambridge, UK, 1992, pp. 139–146.

[57] C. Klein, N.J. Beukes, Geochemistry and sedimentology of a facies transition from limestone to iron-formation deposition in the Early Proterozoic Transvaal Supergroup, South Africa, Econ. Geol. 84 (1989) 1733–1774.

[58] A.J. Kaufman, J.M. Hayes, C. Klein, Primary and diagenetic controls of isotopic compositions of iron-formation carbonates, Geochim. Cosmochim. Acta 54 (1990) 3461–3473.